Biophysical Journal, Volume *113*

Supplemental Information

Physical Mechanisms Driving Cell Sorting in *Hydra*

Olivier Cochet-Escartin, Tiffany T. Locke, Winnie H. Shi, Robert E. Steele, and Eva-Maria S. Collins

Supplementary movies

Movie S1.Time lapse imaging of sorting of a watermelon aggregate. The ectoderm is shown in green and the endoderm in magenta. The change in projected area is a signature of rounding up which occurs on a longer time scale than cell sorting.

Movie S2. Representative rounding up experiment on an endoderm tissue piece.

Movie S3. Long term fusion of two endoderm tissue pieces.

Movie S4. Long term behavior of an aspirated endoderm tissue piece.

Movie S5. Comparison of fusion success rate between endoderm and ectoderm tissue pieces in similar conditions.

Movie S6. Representative sorting simulation. A 2d slice in the middle of the aggregate and a 3d view are shown side by side. Axes are in pixels.

Movie S7. 3d views of simulations of fusion of two pieces of the same cell type, axes in pixels.

Movie S8. View of a 2d slice of a simulation showing the engulfment of an endoderm tissue piece by an ectoderm one. Axes in pixels.

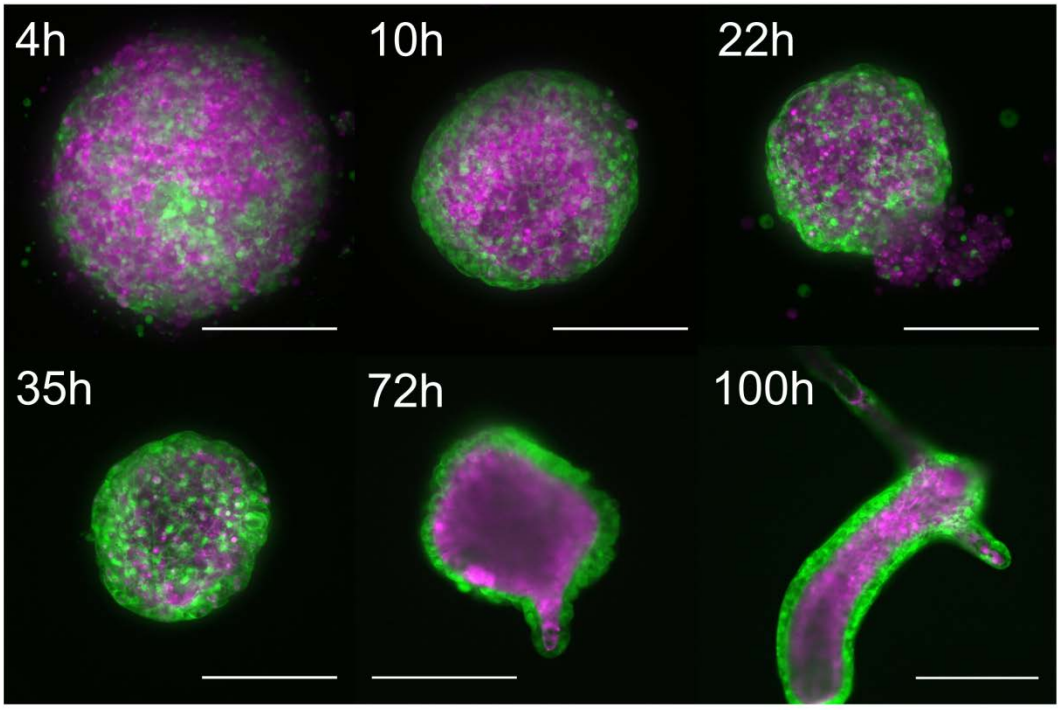

Figure S1. Image sequence of a watermelon aggregate all the way to full regeneration. Scales bars: 200μm except in the last panel where it is 500μm.

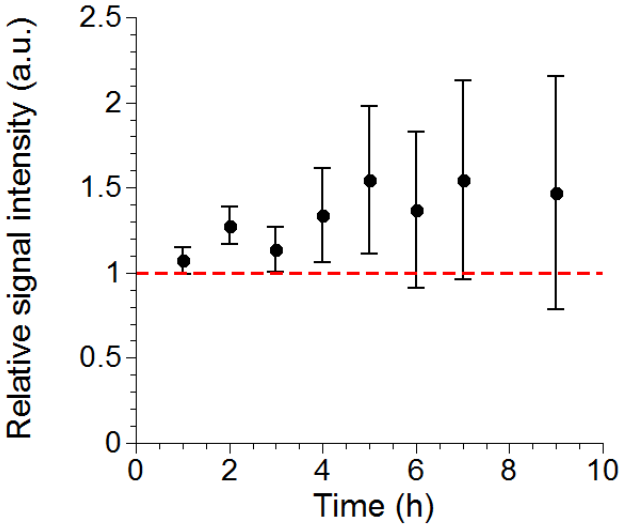

Figure S2. Quantification of laminin levels from antibody stainings. The signal intensity is normalized to a negative control without primary antibody. Thus, a value of 1 represents an absence of signal and a value of 1.5 represents a signal 50% brighter than this negative control. Notably, there is no significant increasing trend in the amount of signal observed over the course of sorting.

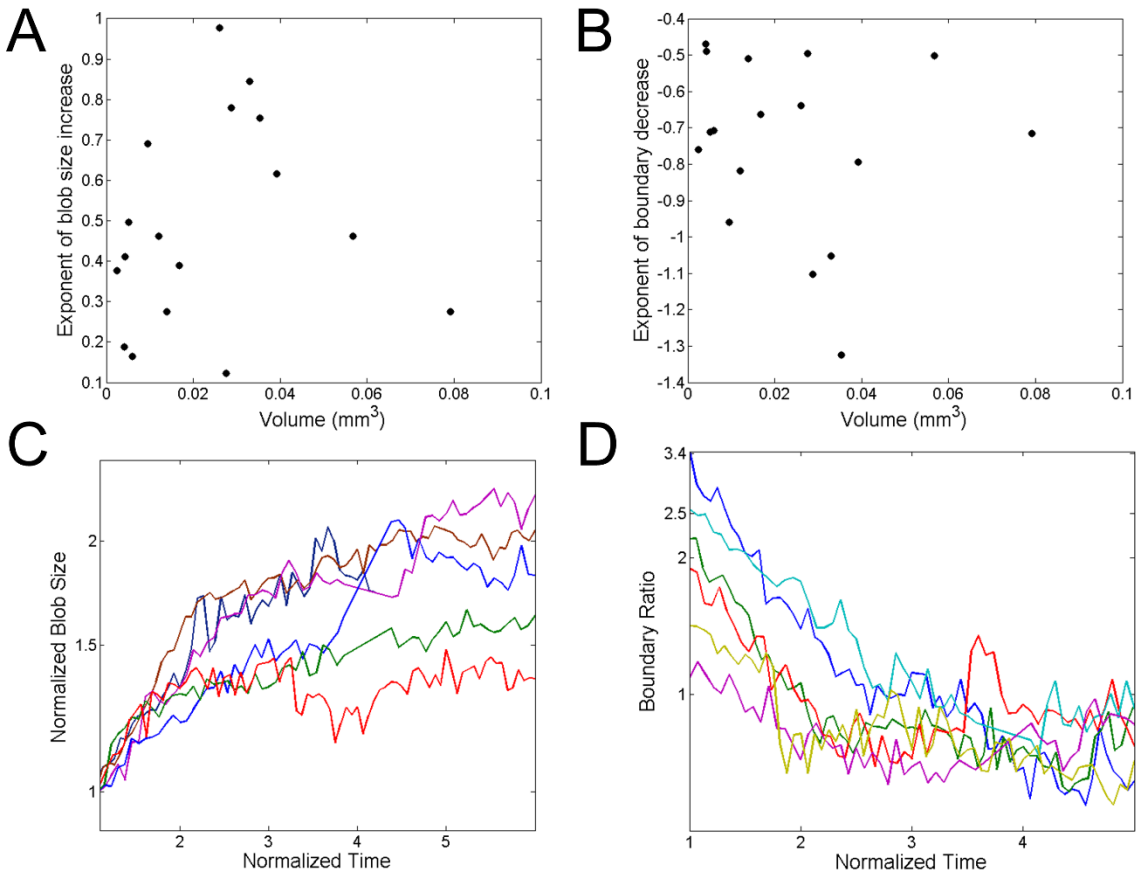

Fig S3. Exponents of blob size increase (A) and boundary decrease (B) as a function of aggregates final sizes in experiments (n=17 from 5 technical replicates). (C-D) Semilog plots of blob size (C) and boundary length (D) of the data shown in Fig 1.

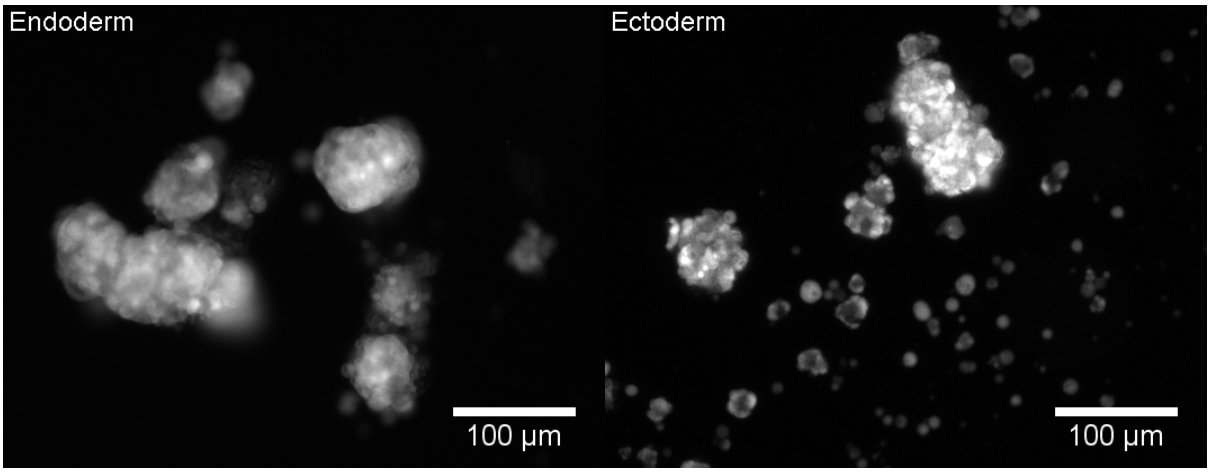

Figure S4. Cell clusters obtained by centripetal aggregation of single cells for endoderm and ectoderm. The obtained clusters have projected areas of 2554±1183µm^2 and 606±273µm^2 (mean±SEM, n=7 and 30 respectively) for endoderm and ectoderm.

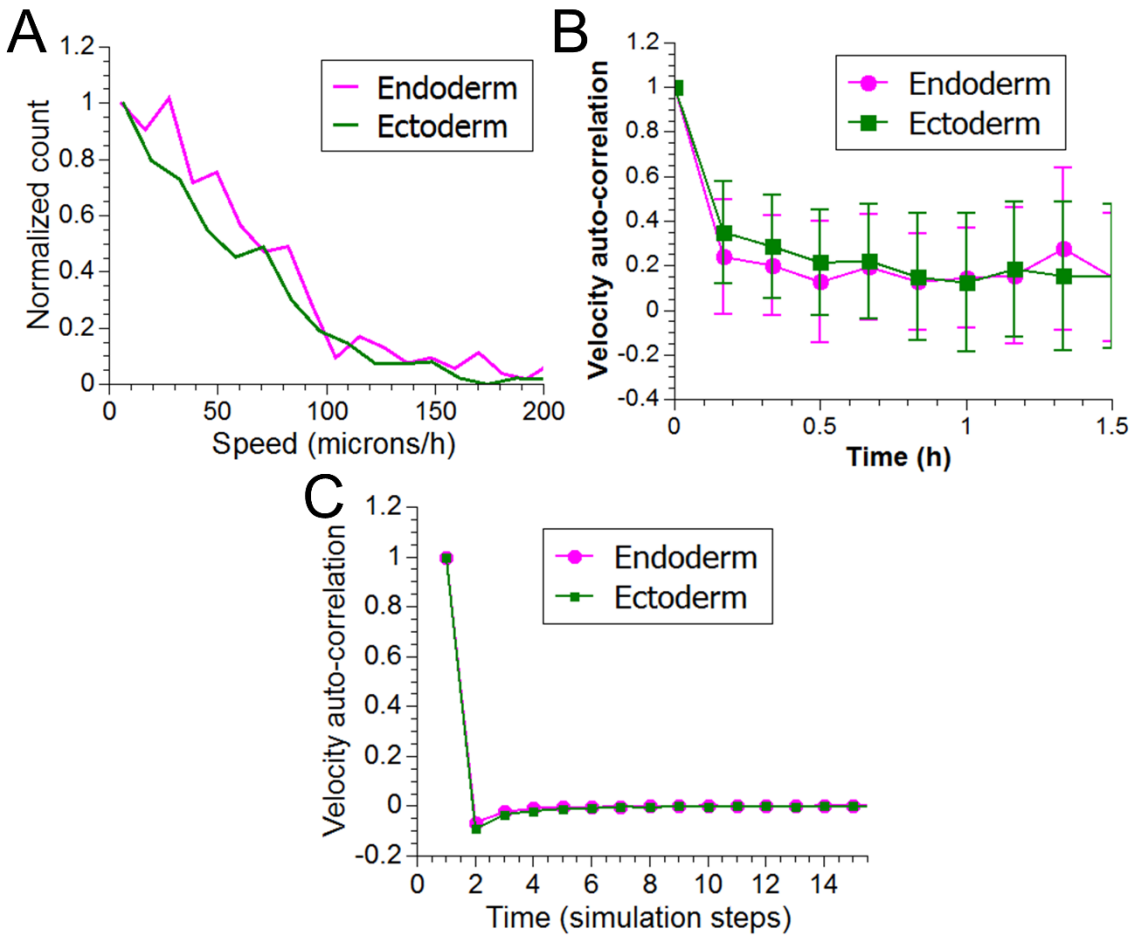

Figure S5. Speed distributions (A) and velocity auto-correlation functions (B) from single cell tracking during one representative experiment. (C) Velocity auto-correlation function from one simulation.

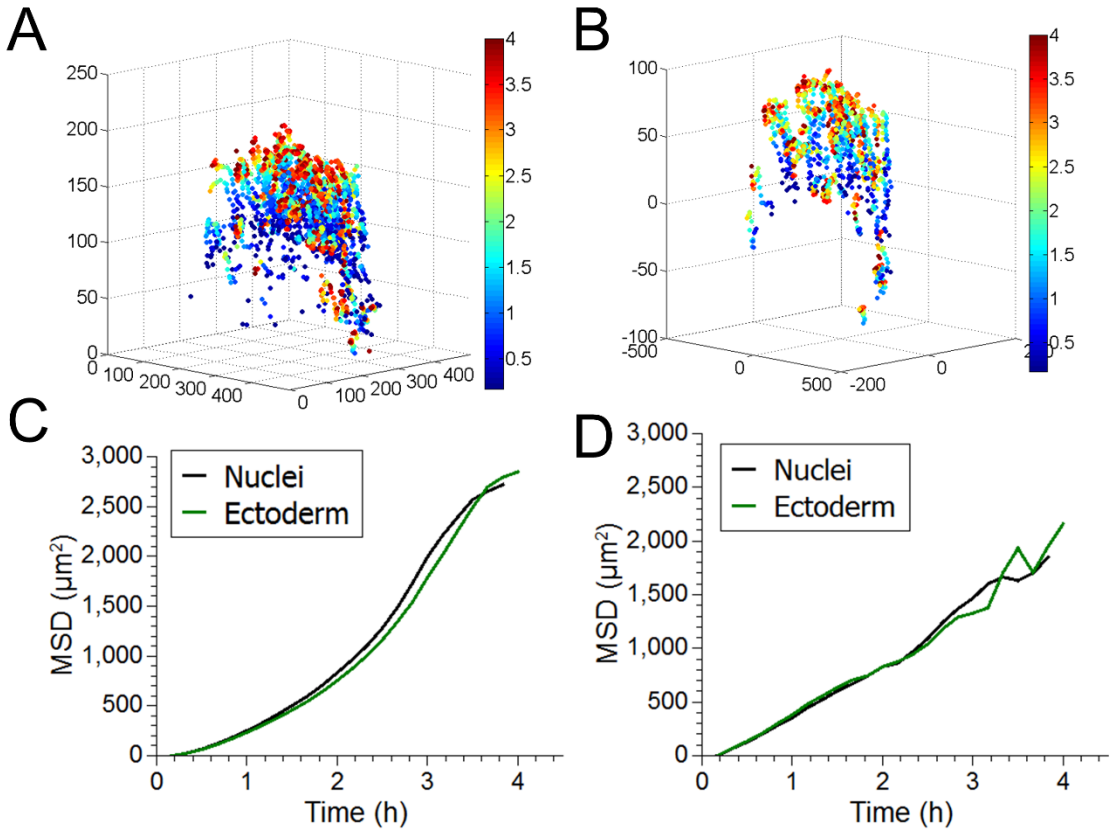

Figure S6. (A-B) Nuclear tracks color coded by time (in h) before (A) and after (B) center of mass correction. (C-D) Corresponding mean square displacements of all nuclei (black) and ectodermal cells (green) before (C) and after (D) center of mass correction.

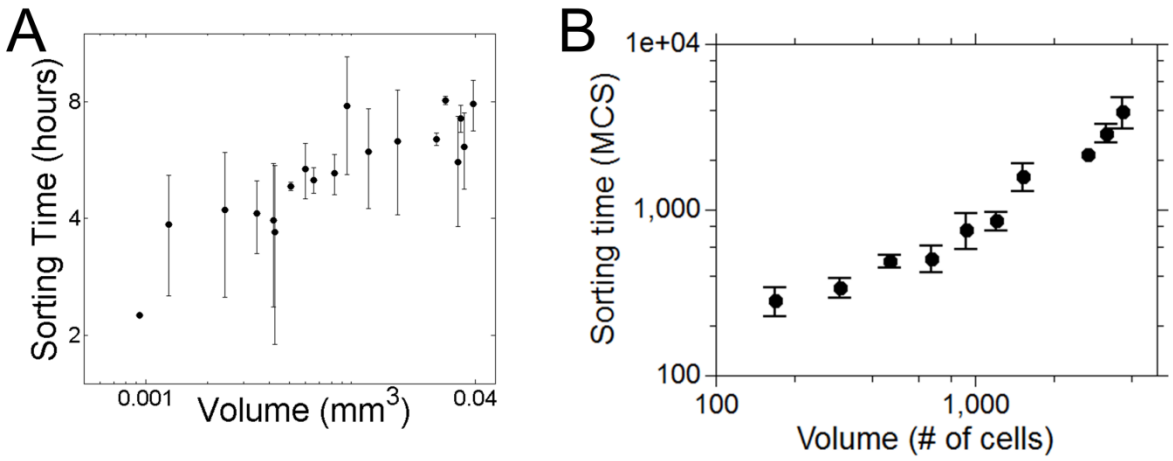

Figure S7. Log-log plot of sorting times as a function of aggregate size for experiments (A) and simulations (B). In (A), each point represents a single aggregate (n=17 from 5 technical replicates)

and error bars represent uncertainty from two different visual inspections. In (B), each point represents the average of three separate simulations and error bars represent standard deviation.

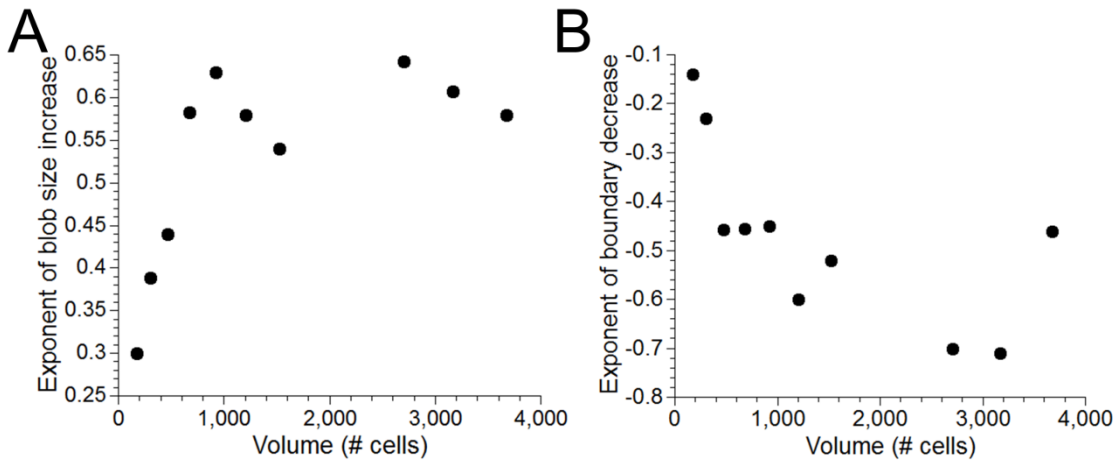

Figure S8. Exponents of blob size increase (A) and boundary decrease (B) as a function of final aggregate sizes in simulations. Each data point is obtained from the averaged dynamics of three simulations performed at the same size. No effect of size was observed except for the three smallest sizes that were excluded from the averages shown in the main text.

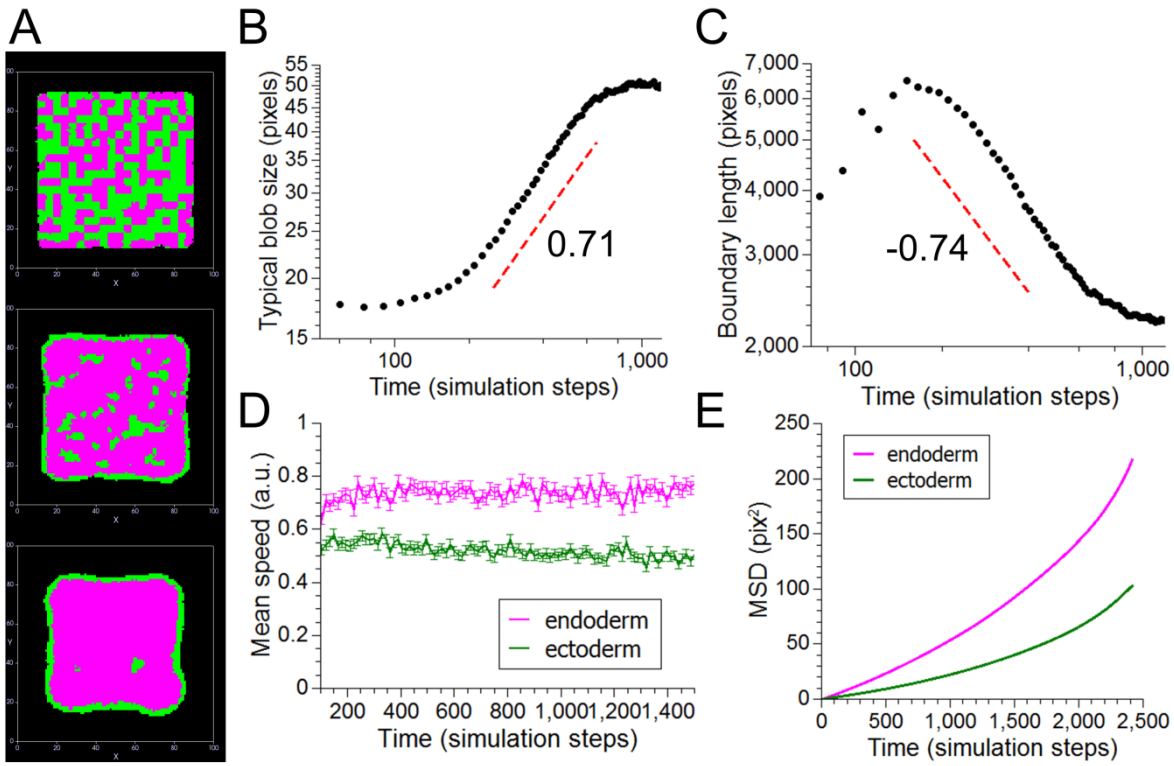

Figure S9. Dynamics of sorting with differential motility. A) Snapshots of sorting at different time points (0, 300 and 900MCS). B) Log-log plot of blob size as a function of time for the average of six different simulations. The dashed red line shows the behavior of a power law with exponent 0.71. C) Log-log plot of boundary length as a function of time for the average of six different simulations. The dashed red line shows the behavior of a power law with exponent -0.74. D) Measurement of speeds over time for a representative simulation. E) Mean square displacement of the same simulation as in D).

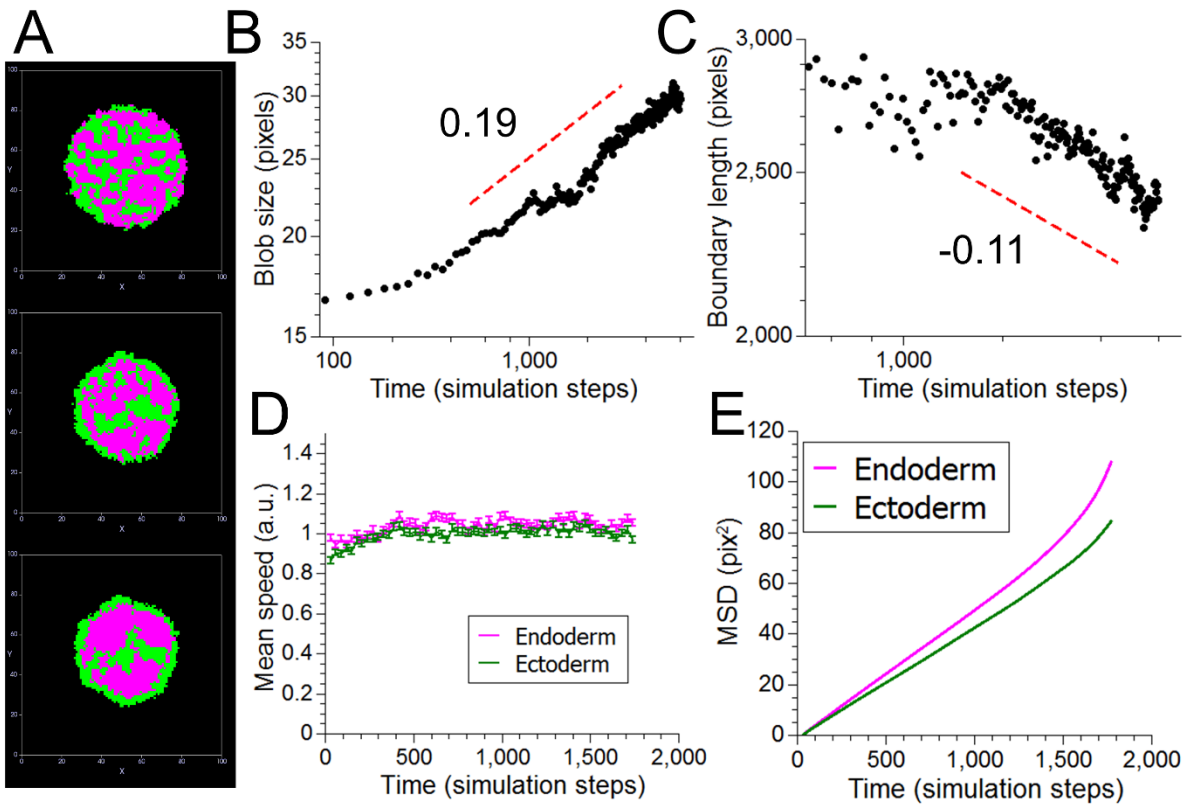

Figure S10. Simulations of sorting from spherical initial conditions. A) Snapshots of sorting at different time points (0, 300 and 900MCS). B) Log-log plot of blob size as a function of time for the average of six different simulations. The dashed red line shows the behavior of a power law with exponent 0.19. C) Log-log plot of boundary length as a function of time for the average of six different simulations. The dashed red line shows the behavior of a power law with exponent -0.11. D) Measurement of speeds over time for a representative simulation. E) Mean square displacement of the same simulation as in D).

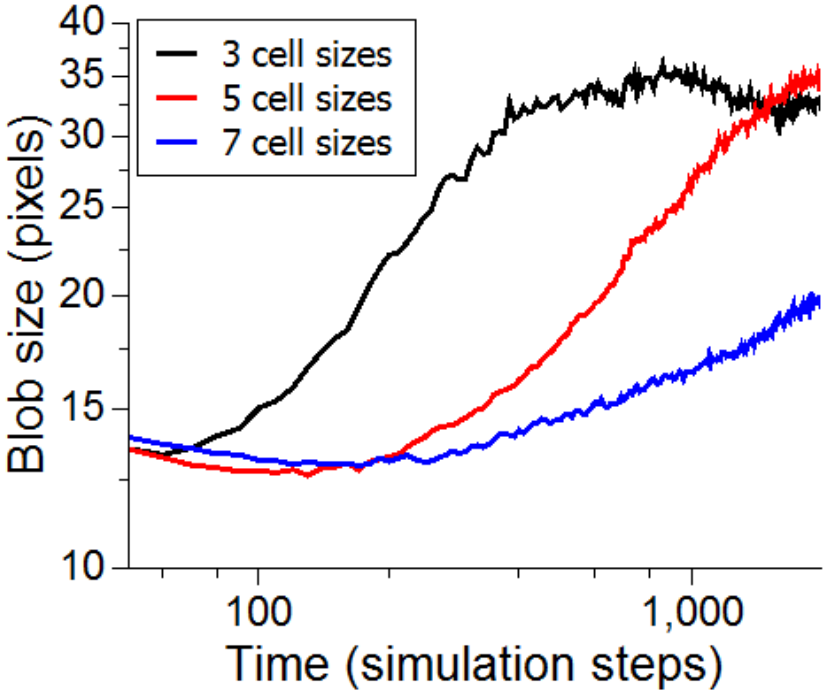

Figure S11. Log-log plot of blob size as a function of time for three different thicknesses (3,5 and 7 cell sizes) for simulated aggregates. Each curve is the mean of six simulations with 80*80 pixels large aggregates.

Measurement	**Method**	**Endoderm**	**Ectoderm**	**n=**
Elastic modulus	Parallel plate compression (41)	4.4 +/- 0.1 kPa	4.9 +/- 0.7 kPa	88 and 83
Viscosity	Micro-aspiration	3.7 ± 2.0 10^4 Pa.s	4.8 +/- 1.9 10^4 Pa.s	10 and 9
Surface tension	Micro-aspiration	13.4 +/- 4.0 dyn/cm	9.1 +/- 2.6 dyn/cm	14 and 13
Surface tension	Rounding	3.3 +/- 2.7 dyn/cm	1.5 +/- 0.9 dyn/cm	17 and 15

Table S1. Rheological measurements, values are mean±STD.